Paper:

Development of Earthquake-Induced Building Damage Estimation Model Based on ALOS/PALSAR Observing the 2007 Peru Earthquake

Masashi Matsuoka* **and Miguel Estrada****

*Interdisciplinary Graduate School of Science and Engineering, Tokyo Institute of Technology
Nagatsuta 4259-G3-2, Midori-ku, Yokohama 226-8502, Japan
E-mail: matsuoka.m.ab@m.titech.ac.jp
**Japan-Peru Center for Earthquake Engineering and Disaster Mitigation (CISMID), National University of Engineering
Av. Túpac Amaru 1150, Lima 25, Peru
E-mail: estrada@uni.edu.pe
[Received November 11, 2012; accepted December 14, 2012]

With the aim of developing a model for estimating building damage from synthetic aperture radar (SAR) data in the L-band, which is appropriate for Peru, we propose a regression discriminant function based on field survey data in Pisco, which was seriously damaged in the 2007 Peru earthquake. The proposed function discriminates among damage ranks corresponding to the severe damage ratio of buildings using ALOS/PALSAR imagery of the disaster area before and after the earthquake. By calculating differences in and correlations of backscattering coefficients, which were explanatory variables of the regression discriminant function, we determined an optimum window size capable of estimating the degree of damage more accurately. A normalized likelihood function for the severe damage ratio was developed based on discriminant scores of the regression discriminant function. The distribution of the severe damage ratio was accurately estimated, furthermore, from PALSAR imagery using data integration of the likelihood function with fragility functions in terms of the seismic intensity of the earthquake.

Keywords: severe damage ratio, ALOS/PALSAR, the 2007 Peru earthquake, likelihood function, backscattering coefficient, data integration

1. Introduction

Satellite remote sensing is being increasingly used for quick assessment of the impact of natural disasters occurring worldwide [1]. The size and location of affected areas are estimated, for example, by comparing post- with pre-event imagery, since satellites orbiting the earth often observe pre-event states at many locations [2, 3]. In recent years, the resolution of optical sensors on board satellites has increased to approximately 60-cm ground resolution, which allows us to visually interpret the shapes of buildings and the states of large-scale damage [4, 5]. If a disaster strikes an extensive area, however, it takes considerable time to assess damage through visual interpretation, making it impractical for rapid assessment. In addition, because damage estimation by visual interpretation inherently involves variability attributable to differences in the perception of the interpreter, there are problems with standardization and the general versatility of the method. In order to overcome such disadvantages, attempts have involved the use of a network of many volunteers to visually interpret building damage in an extensive disaster area, namely, crowdsourcing [6]. There is a need to improve the accuracy of the visual interpretation of damage. To this end, engineers with knowledge and experience in interpreting aerial imagery should prepare instruction manuals that allow nonexperts to participate in this visual interpretation of damage, and should also establish a screening technique to eliminate unreliable data. Such a system of exploiting the enormous human resources outside the disaster area is expected to become a technology used in responding to major disasters.

Synthetic aperture radar (SAR), a type of "remote sensing sensor," observes the surface of the earth day and night, regardless of weather. If the visual interpretation of damage from SAR imagery is practicable, it will complement visual interpretation from optical sensor imagery. Unlike optical sensor images, which look like photographs, however, SAR imagery represents the intensity of microwave backscattering from the ground surface and is unfamiliar to nonexperts. It is therefore difficult to visually interpret damage from SAR images by crowdsourcing. It is thus expected that damage from SAR imagery will be extracted by computer-based image processing [7–10]. Estimation models for building damage ratios have therefore been proposed [11–13] based on C-band (wavelength: 5.7 cm) SAR imagery in which building damage data obtained from detailed field surveys conducted after the Kobe earthquake in 1995 were used as ground-truth data and the applicability of one of the models used for damage extraction in other earthquakes

1. This paper is translated with revision from the paper published in the Journal of Japan Association for Earthquake Engineering, Vol.12, No.6, pp. 36-49 in Japanese.

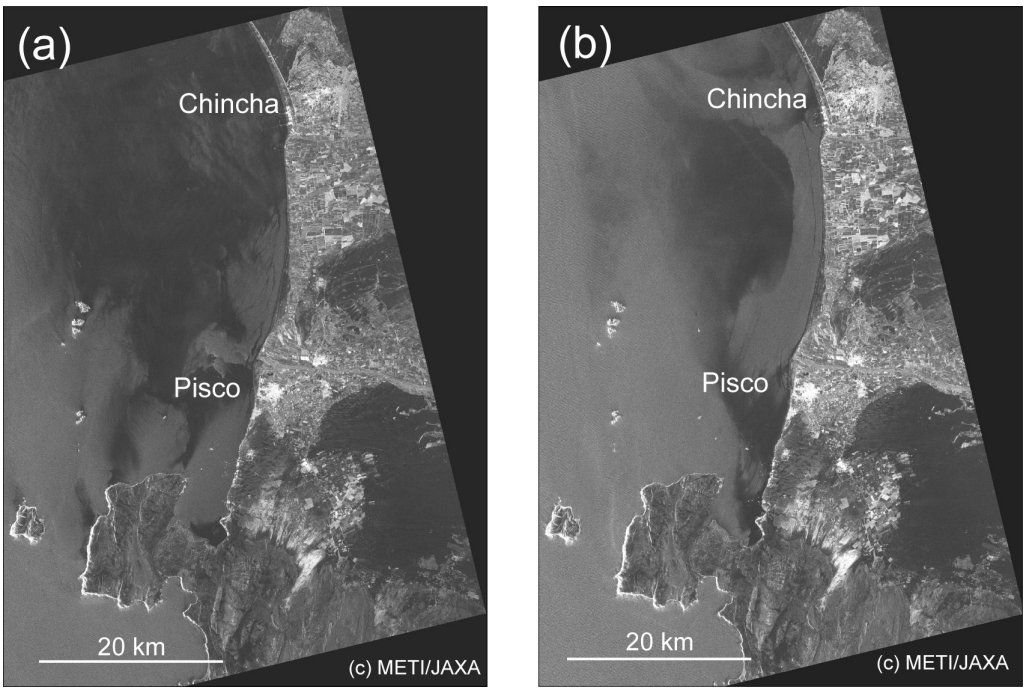

Fig. 1. PALSAR imagery obtained before and after the 2007 Peru earthquake: (a) July 12, 2007; (b) August 27, 2007.

occurring in various countries and regions was investigated [12]. The model was further improved so that it was also applicable to imagery obtained by JERS-1/SAR and ALOS/PALSAR (PALSAR imagery), which is L-band (wavelength: 23 cm) SAR mounted on Japanese satellites. It was then applied to PALSAR imagery obtained in the 2007 Peru earthquake and the 2008 Wenchuan, China, earthquake [13]. It was found from comparison with damage assessment reports of these earthquakes, etc., that local damage areas could not be detected because the model was based on the ground-truth data of the 1995 Kobe earthquake. In other words, it was demonstrated that application of the model to other countries and regions, which have urban structures, building types, and damage situations different from Japan, gave inaccurate results [13].

Following procedures reported in our previous papers [11, 13], this paper develops a model for estimating a severe damage ratio of buildings that reflects the building types and damage situation in Peru. The model is an estimation model for severe damage ratio optimized for Peru because it is based on PALSAR imagery of Pisco after the 2007 Peru earthquake and on building damage data obtained from field surveys. Specifically, an optimum window size for image processing was determined and a normalized likelihood function for the severe damage ratio was derived. The model was used, furthermore, to estimate damage by integrating image data with seismic intensity data and comparing results with the actual damage to be checked.

2. PALSAR Images and Field Survey Data

2.1. Indices Obtained from PALSAR Imagery and Image Processing

On August 15, 2007, an earthquake measuring M8.0 with an epicenter 40 km northwest of Chincha, Peru. The city of Pisco in the Ica Region and the surrounding area were devastated by the earthquake, which left more than 500 people dead or missing and completely destroyed more than 35,000 buildings. About 2 weeks after the earthquake, high-resolution PALSAR imagery of the coastal area was obtained. **Figs. 1(a)** and **(b)** shows images obtained on July 12, 2007, before the earthquake and on August 27, 2007, after the quake. The nominal ground resolution was approximately 10 m and the image pixel size 12.5 m.

Two indices – the difference between post- and pre-earthquake images and the correlation coefficients of backscattering coefficients – were calculated from pre- and post-earthquake PALSAR images. Following the accurate positioning of both pre- and post-event images, a speckle reduction filter was applied to each image [14], then differences and correlation coefficients were calculated from Eqs. (1) and (2), below. The difference is obtained by subtracting the average value of the backscattering coefficient within an $N \times N$ pixel window of the pre-event image from that of the post-event image. The correlation coefficient is also calculated from the same $N \times N$ pixel window. Analysis results from the 1995 Great Hanshin-Awaji Earthquake Disaster (widely called the Kobe earthquake) showed that differences (after – before) yielded negative values, with the spatial distribution of backscattering coefficients decreasing with building damage and as compared with that in pre-event im-

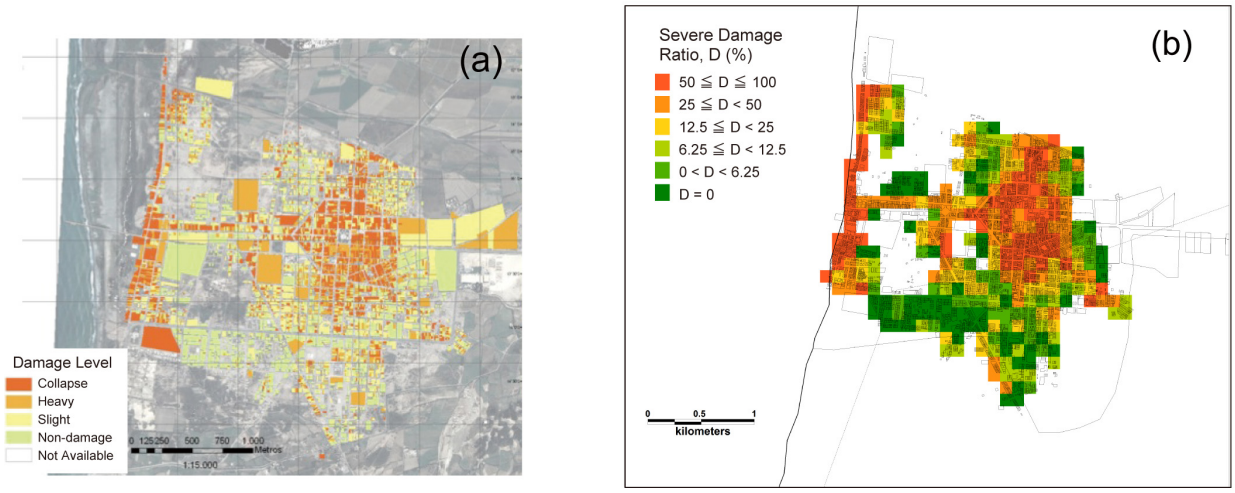

Fig. 2. Building damage data at Pisco based on a field survey. (a) Damage level by lot (Estrada et al., 2008). (b) Distribution of the severe damage ratio.

agery, resulting in an overall decrease in correlation coefficient [10].

$$d = 10 \cdot \log_{10} \bar{I}a_i - 10 \cdot \log_{10} \bar{I}b_i \quad \ldots\ldots (1)$$

$$r = \frac{N \sum_{i=1}^{N} Ia_i Ib_i - \sum_{i=1}^{N} Ia_i \sum_{i=1}^{N} Ib_i}{\sqrt{\left(N \sum_{i=1}^{N} Ia_i^2 - \left(\sum_{i=1}^{N} Ia_i \right)^2 \right) \cdot \left(N \sum_{i=1}^{N} Ib_i^2 - \left(\sum_{i=1}^{N} Ib_i \right)^2 \right)}} \quad \ldots\ldots (2)$$

where d represents the difference in backscattering coefficients [dB], r is the correlation coefficient, and N is the number of pixels within the window to be calculated. Ia_i and Ib_i represent the i^{th} pixel values of post- and pre-event images, respectively, and $\bar{I}a_i$ and $\bar{I}b_i$ represent average values of $N \times N$ pixels surrounding the i^{th} pixel.

2.2. Severe Damage Ratio of Buildings Based on Field Survey Data

The target area of the damage estimation model is the city of Pisco. Damage data used in this study were collected by members of the Japan-Peru Center for Earthquake Engineering and Disaster Mitigation (CISMID), National University of Engineering, Peru. CISMID personnel performed detailed on-site investigations of buildings in more than 10,000 lots just after the earthquake [15] and this was considered to be the most reliable data on the Peru earthquake. Investigation items included building lot codes, building use, structure types, floor number, and damage level, all of which were combined with geographic information system (GIS) data. Approximately 97% of buildings in the area were masonry structures – 18% adobe structures and 79% burnt brick structures – which are comparatively weak and are prone to collapse in general. In the earthquake, adobe buildings were greatly damaged. Lots and buildings were mostly in a one-to-one correspondence. For multiple buildings located on large lots, information on the most damaged building was recorded. **Fig. 2(a)** shows the distribution of damage levels by lot based on the field survey in Pisco.

Table 1. Range of severe damage ratio and median values for damage ranks.

Damage Rank	Severe Damage Ratio D (%)	Median Value (%)
C1	$D = 0$	0.0
C2	$0 < D < 6.25$	3.13
C3	$6.25 \leq D < 12.5$	9.38
C4	$12.5 \leq D < 25$	18.75
C5	$25 \leq D < 50$	37.5
C6	$50 \leq D \leq 100$	75.0

Damage levels were classified into the following four: Grave (Serious), Severo (Severe), Leve (Slight), and Sin daño (No damage). Lots that could not be investigated were categorized as "Not available." Grave corresponds to G5 in the classification of the European Macroseismic Scale (EMS-98) [16], Severo to G4 and G3, Leve to G2, and Sin daño to G1. The damage ratio was calculated based on these GIS data. In order to take sizes of lots, including vacant lots, into consideration and to calculate reliable damage ratios, the city of Pisco was split into a grid of 3.75×3.75 arc-seconds (approximately 120-m grid) and estimation was performed only on grids with 10 or more lots. The severe damage ratio of buildings in a grid was calculated as the ratio of the number of Grave to the total number of buildings in the grid. The severe damage ratio was classified into the following six damage ranks: C1, 0% severe damage ratio in a grid; C2, more than 0% and less than 6.25%; C3, 6.25% or more and less than 12.5%; C4, 12.5% or more and less than 25%; C5, 25% or more and less than 50%; and C6, 50% or more. **Ta-**

ble 1 shows the correspondence of damage rank, severe damage ratio and median values. The distribution of the severe damage ratio is shown in **Fig. 2(b)**.

3. Estimation of Severe Damage Ratio Based on Regression Discriminant Function

3.1. Influence of Window Size on Accuracy of Damage Discrimination

In previous studies [10–13], a speckle reduction filter with a 21×21 pixel window was applied to SAR images and differences and correlation coefficients were calculated from a 13×13 pixel window. Although these window sizes suited extraction of the damaged area from 30-m resolution SAR imagery of an area affected by the Kobe earthquake and field survey data in the Hanshin area [10], it was uncertain whether these window sizes would be the optimum for extracting damage in a city in Peru, where building types are different from those in the Hanshin area, with approximately 10-m resolution, which is the same as PALSAR imagery resolution. Accordingly, the change in the accuracy of damage discrimination was examined by varying speckle reduction filter size and calculation window size for Pisco data sets.

The influence of speckle reduction filters was examined first. A Lee filter size [14] that is variable from 3×3 to 51×51 pixels was applied to pre- and post-event images and differences and correlation coefficients were calculated based on Eqs. (1) and (2). Images of differences and correlation coefficients were overlaid on field survey data and 800 pixels were randomly extracted from areas corresponding to each of the six damage ranks shown in **Table 1** (4,800 pixels in total) to create a training sample. For quantitative evaluation of the severe damage ratio, regression discriminant analysis [17] – a method of multiple-group discriminant analysis that uses differences and correlation coefficients of the six damage ranks – was applied. Window sizes of 7×7, 13×13, and 21×21 pixels were examined to calculate differences and correlation coefficients. **Fig. 3** shows the correlation ratio of regression discriminant functions representing the ability to discriminate six damage ranks against the pixel dimension calculated from the size of the speckle reduction filter. In this figure, a larger correlation ratio means better discriminant ability of damage ranks. The relationship between pixel dimension and correlation ratio is slightly complicated because as the size of the filter increases, the correlation ratio decreases, but turns upward at 15×15 pixels. The correlation ratio obtained when the filter size is increased to the largest one of 41×41 pixels is almost the same as that obtained without any filter, however, so it was determined that no filter would be used in this study.

The influence of window size on the accuracy of discrimination was examined next. The correlation ratio of regression discriminant functions was calculated using varying window size from 3×3 to 51×51 pixels to calculate differences and correlation coefficients. **Fig. 4**

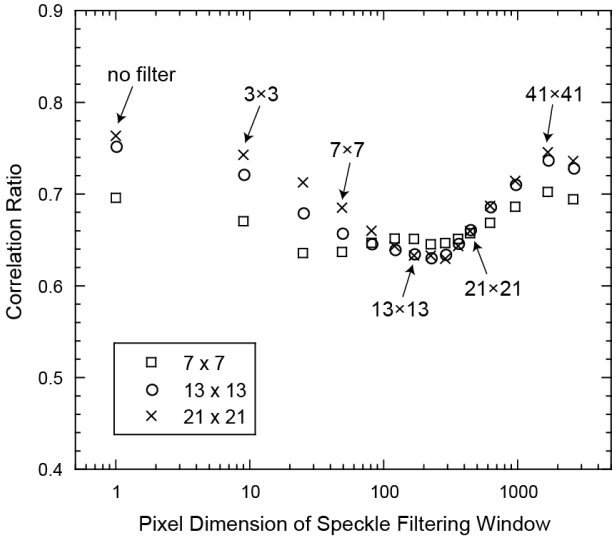

Fig. 3. Relationship between the size of speckle reduction filters and the correlation ratio.

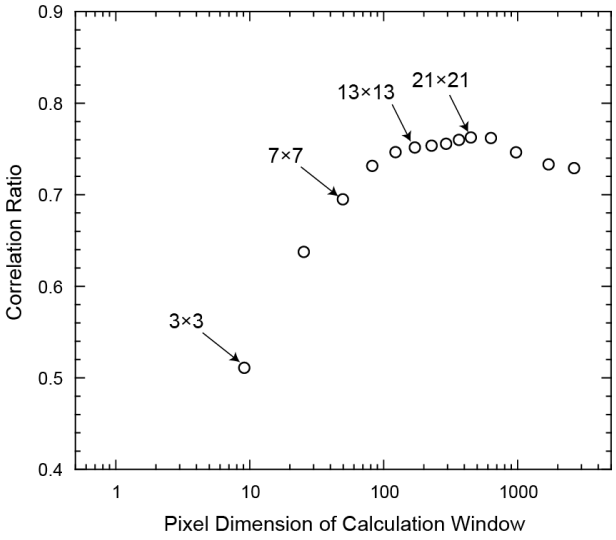

Fig. 4. Relationship between the calculation window size and the correlation ratio.

shows correlation ratio against pixel dimension calculated from window size. Window size increased from 3×3, so the correlation ratio increased, reaching a limit at around 13×13 pixels. This was also found for data sets in the Hanshin area before and after the Kobe earthquake [10]. The reasons why the correlation ratio increases includes the fact that damaged building groups spread to some extent and, in addition, backscattering of each damaged building has a spatial extent. Interestingly, although the pixel size of SAR images in the Hanshin area and Pisco are different, the window size at which the correlation ratio reached a limit was the same, i.e., at around 13×13 pixels. Although this is considered to arise from complex factors such as the fact that different damage situations are involved, the detail remains a challenge to be addressed. It should be noted that although the correlation ratio reached a maximum in **Fig. 4** when

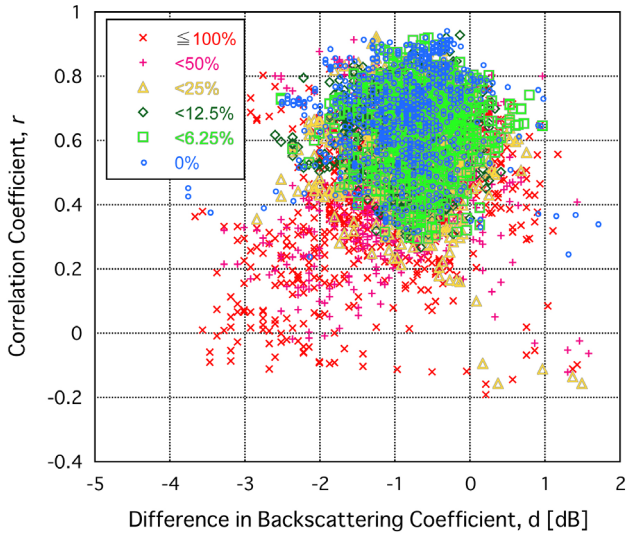

Fig. 5. Relationship between differences in backscattering coefficients and correlation coefficients for damage ranks.

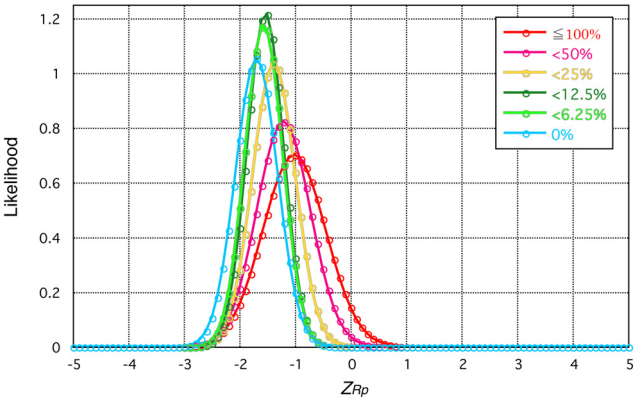

Fig. 6. Normal frequency distribution model of discriminant score Z_{Rp}.

Table 2. Average values and standard deviations in the likelihood function of data in PALSAR intensity imagery.

Damage Rank	Average of Z_{Rp}	Standard Deviation
C1	-1.470	0.323
C2	-1.355	0.291
C3	-1.332	0.281
C4	-1.200	0.331
C5	-1.052	0.415
C6	-0.887	0.484

21×21 pixels were used, the value is almost the same as that for 13×13 pixels. A larger window size, however, does not offer the capability for detecting small spatial changes within a window, so we decided in our study to use a 13×13 pixel window, which was also used in the previous study.

3.2. Derivation of Regression Discriminant Function and Likelihood Function

To calculate difference d and correlation coefficient r, a window size of 13×13 pixels was adopted as the optimum size to interpret damage in Pisco based on the analysis of data sets, and no speckle reduction filter was used. **Fig. 5** shows a scatter diagram by damage rank. The regression discriminant function calculated from the two indices is shown in Eq. (3):

$$Z_{Rp} = -0.089\ d - 2.576\ r \quad \ldots\ldots\ldots \quad (3)$$

where Z_{Rp} represents the discriminant score derived from PALSAR imagery. While coefficients of d and r in discriminant score Z_{Rj} derived from JERS-1/SAR imagery of the Kobe earthquake were -1.277 and -2.729, respectively [13], coefficients derived here from PALSAR imagery of Pisco were -0.089 and -2.576. These coefficients indicate the degree of influence of d or r on the discriminant score. Comparison between the Hanshin area and Pisco demonstrated that the coefficient of r, the correlation coefficient, was almost the same in the two regions, but the coefficient of d, the difference in backscattering coefficients, of Pisco was small, or approximately zero, compared with that of the Hanshin area. The influence of d on discrimination of the damage rank in Pisco is therefore negligible.

Next, a likelihood function for estimating the severe damage ratio from discriminant score Z_{Rp} is formed following procedures similar to those in the previous study [11, 13]. The likelihood function in this study means the probability of being in each damage rank when Z_{Rp} is given. Specifically, the frequency distribution of Z_{Rp} of 800 randomly extracted pixels from each damage rank is modeled as a normal distribution. **Fig. 6** shows normal distribution models (likelihood function). **Table 2** shows average values and standard deviations of Z_{Rp} for individual damage ranks. The higher the damage rank, the larger the discriminant score Z_{Rp}. Because distribution curves of some damage ranks cross in regions with low discriminant scores, however, discrimination in areas with low damage ranks is not possible. **Fig. 7** shows normalized likelihood functions in which the sum of the likelihood of all damage ranks in **Fig. 6** becomes 1.0. For regions where Z_{Rp} is -2.2 or less, a constant value obtained by extrapolating the value at $Z_{Rp} = -2.2$ is used in order to avoid reversing the sequence of the severe damage ratio caused by distribution curves crossing. Average values and standard deviation of the estimated severe damage ratio against discriminant score Z_{Rp} are thus obtained from median values of the damage rank in **Table 1** and the distribution shown in **Table 2** and **Fig. 7**. **Fig. 8** shows curves of average values and average values $\pm$ standard deviation of the severe damage ratio estimated from Z_{Rp}. The severe damage ratio increases with increasing Z_{Rp}. Because the discriminant score was adjusted to make the constant term zero, relative positions on the horizontal axis in **Fig. 8** are arbitrary. Taking this into account, the normalized likelihood function derived from field survey data and PALSAR imagery of Pisco gives a high severe damage ratio

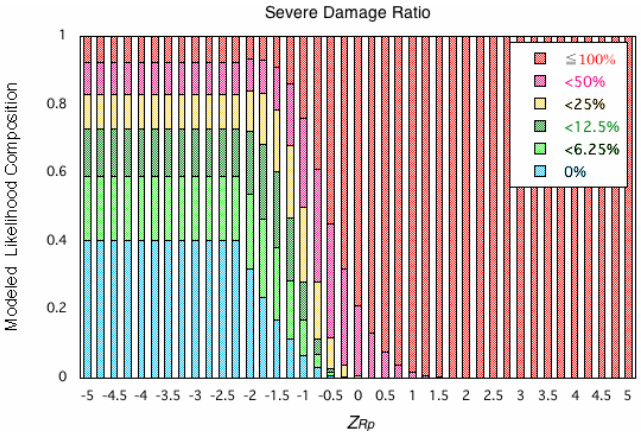

Fig. 7. Normalized likelihood function of discriminant score Z_{Rp}.

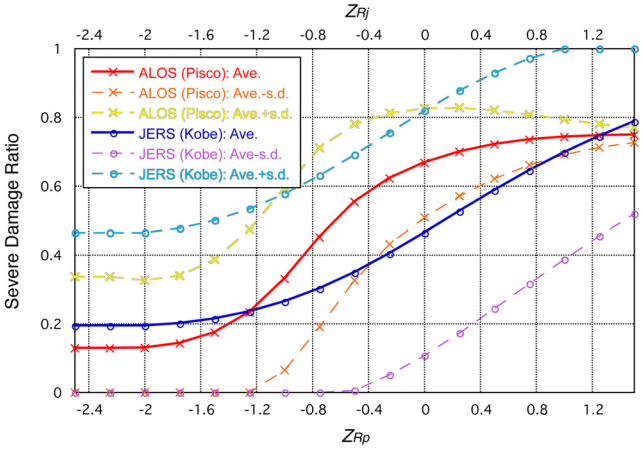

Fig. 8. Relationship between the severe damage ratio (average values and standard deviations) and the discriminant scores of Pisco Z_{Rp} and Hanshin Z_{Rj}.

(average value) in regions with low discriminant scores compared with that derived from field survey data and JERS-1/SAR imagery of the Hanshin area [13] (shown together in **Fig. 8**). It also indicates that small changes in backscattering characteristics have a large influence on the estimation of the severe damage ratio. This could be influenced by differences in building damage situations between Pisco and the Hanshin area.

Figure 9 shows the Z_{Rp} distribution obtained from pre- and post-earthquake PALSAR images, and **Fig. 10** shows the severe damage ratio (average values) estimated from Z_{Rp}. Z_{Rp} values and the severe damage ratio are slightly larger at the center of Pisco. It should be noted that the target area is restricted to urban areas where the cardinal effect can be expected, therefore, areas whose backscattering coefficients are small (-5 dB or under) in pre-event images are masked. The distribution of the severe damage ratio of Pisco city estimated based on PALSAR imagery agrees well with field survey data. Areas with high severe damage ratios are found in sections of farmland, however, because they are not adequately masked owing to variations in backscattering characteristics caused by vegetation.

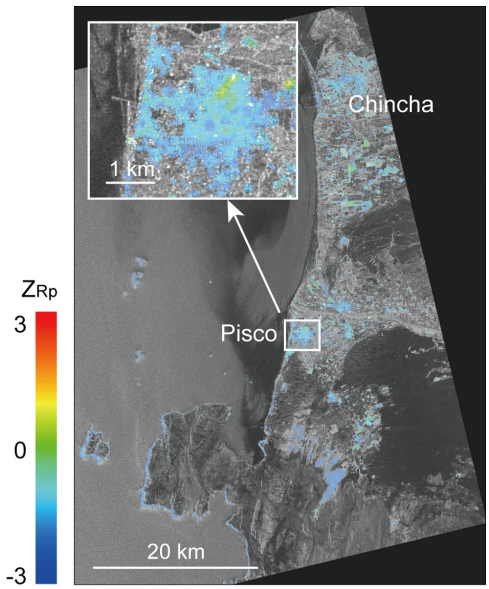

Fig. 9. Discriminant score Z_{Rp} estimated from PALSAR imagery.

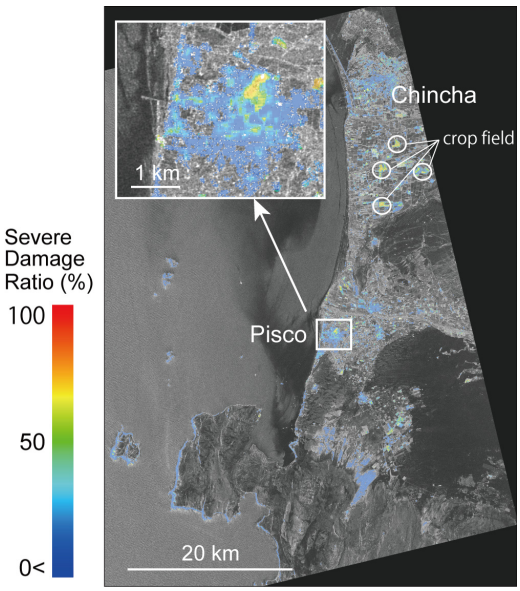

Fig. 10. Severe damage ratio of buildings estimated from the normalized likelihood function (average values).

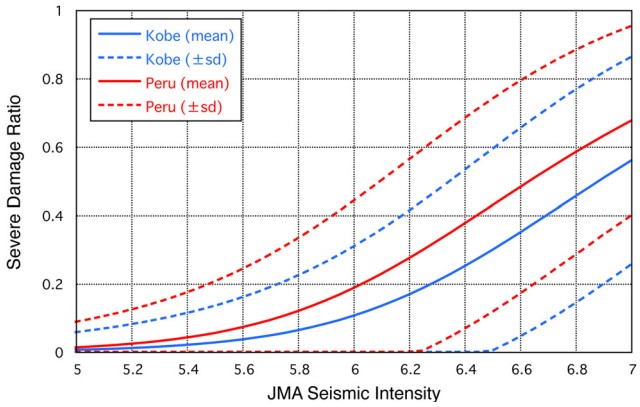

Fig. 11. Relationship between seismic intensity and average values and standard deviations in the fragility function.

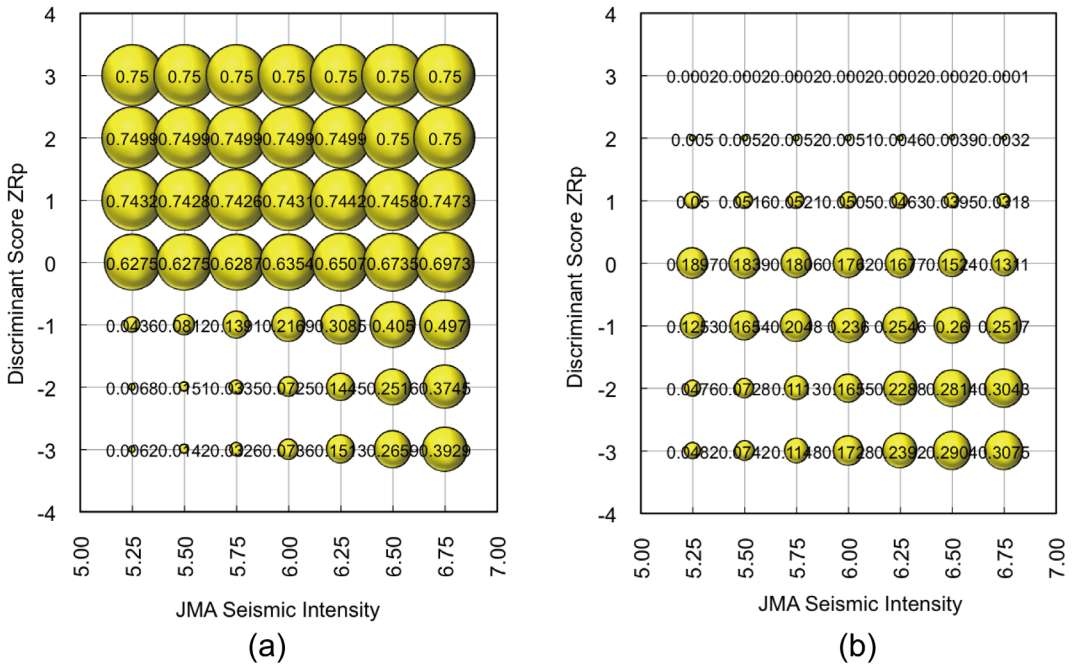

Fig. 12. Estimated severe damage ratio obtained by data integration of PALSAR imagery and seismic intensity data: (a) average values, (b) standard deviations.

4. Severe Damage Ratio Estimation by Integration with Seismic Intensity Data

In a case where only PALSAR imagery is used and $Z_{Rp} < -2.2$, distributions overlap as shown in **Fig. 6** and contain only slightly more information than complete noninformation. In other words, the average severe damage ratio was 13.0% with a standard deviation of 21.0, compared to an average severe damage ratio of 35.4% and a standard deviation of 31.2% when an equal probability of $1/6$ is given for each damage rank. As is shown in **Fig. 10**, a severe damage ratio of approximately 20% is estimated even in broadly undamaged areas. Seismic intensity data is therefore used as supplementary data for highly accurate estimation in all regions, including regions of low severe damage ratio. A fragility function in terms of seismic intensity data has been established based on data obtained from the Kobe earthquake [11]. An improved fragility function that considers the fragility of masonry buildings in Peru has also been developed [13]. **Fig. 11** shows the fragility function for Peru used in this study and that for the Hanshin area for comparison. It corresponds roughly with previous fragility functions [18, 19]; the severe damage ratio of buildings in Peru becomes higher than that in the Hanshin area if buildings are affected by earthquakes of the same seismic intensity.

In line with the work of Nojima et al. [11], Bayesian updating theory has been used to improve the accuracy of estimating the severe damage ratio. It does so by integrating PALSAR imagery Z_{Rp} with seismic intensity data. Specifically, the probability of being in each damage rank is updated by multiplying the probability of being in each damage rank when seismic intensity data is given with the normalized likelihood of Z_{Rp} of each damage rank (equivalent to the probability of being in each damage rank when Z_{Rp} is given), and then normalizing (that is, constraining the sum of probabilities to be one) [11]. **Figs. 12(a)** and **(b)** shows average values and standard deviations in the severe damage ratio based on the probability updated for the $7 \times 7 = 49$ combinations of the two indices. Compared with Kobe earthquake results [13], seismic intensity data contribute to estimating the severe damage ratio where Z_{Rp} of SAR imagery is low, so the severe damage ratio increases steeply and the seismic intensity data contribution is nearly zero where SAR imagery Z_{Rp} is high.

U.S. Geological Survey (USGS) ShakeMap [20] was used for earthquake seismic intensity data. Peak Ground Velocity distribution data from ShakeMap [21] was converted by Fujimoto and Midorikawa [22] into measured seismic intensity, and is shown superimposed on PALSAR imagery in **Fig. 13**. Large shaking of 6− to 6+ on the Japan Meteorological Agency (JMA) seismic intensity scale is found all over the image. The result of estimating the severe damage ratio by data integrating discriminant score Z_{Rp} data obtained from PALSAR imagery (**Fig. 9**) and measured seismic intensities (**Fig. 13**) is shown in **Fig. 14(a)**. An enlarged view of the Pisco area is shown in **Fig. 14(b)**. Because built-up area is the target, areas with backscattering coefficients of −5 dB or less are masked. **Fig. 15** shows enlarged views in the Pisco area of (a) distribution of the severe damage ratio investigated by the field survey, (b) the same distribution estimated from PALSAR imagery alone, and (c) the same distribution based on the data integration of PALSAR imagery and seismic intensity data. Distribution of the severe damage ratio estimated based on the data integration

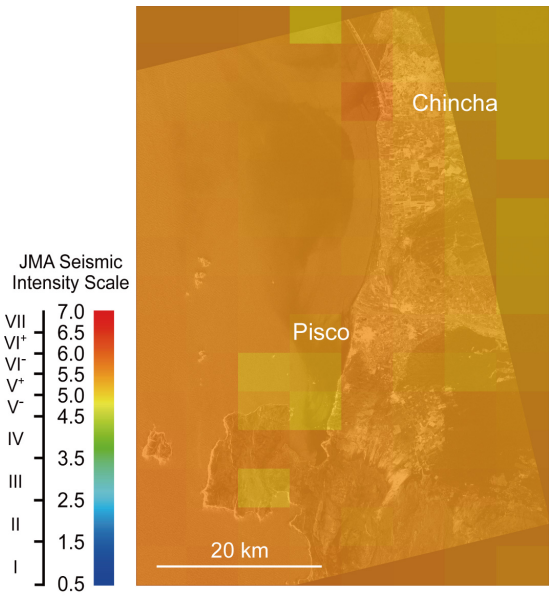

Fig. 13. Distribution of measured seismic intensity estimated from ShakeMap.

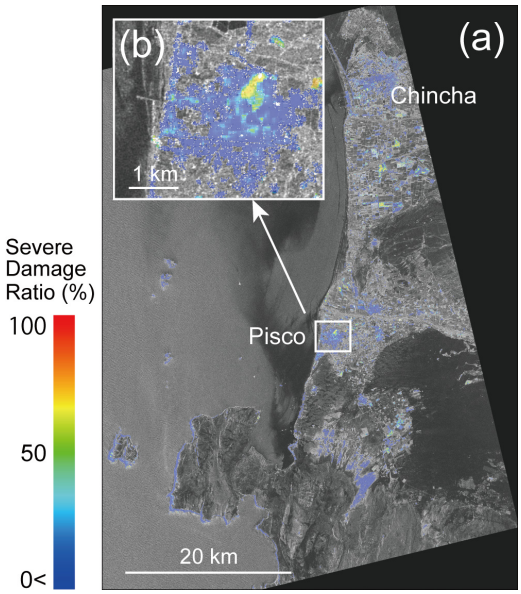

Fig. 14. Estimated severe damage ratio obtained by data integration of PALSAR imagery and seismic intensity data (average values).

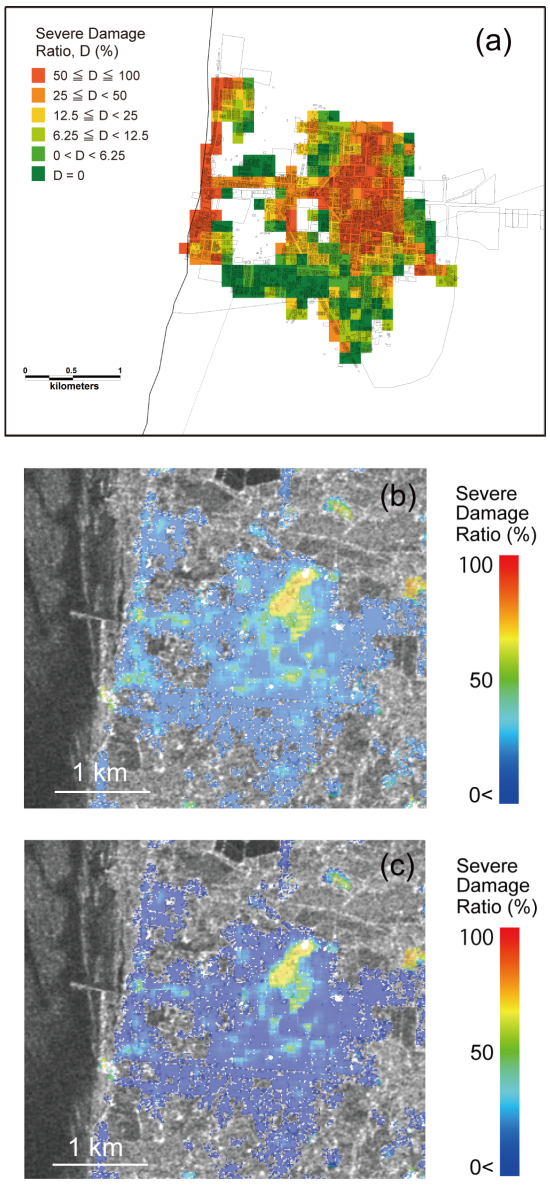

Fig. 15. Comparison of distribution maps of the severe damage ratio in Pisco (enlarged views): (a) field survey, (b) estimation based on PALSAR imagery alone, and (c) estimation based on the data integration of PALSAR imagery and seismic intensity.

of PALSAR imagery and the seismic intensity data is in good agreement with the distribution based on the field survey, especially in areas with a high severe damage ratio in the central part of Pisco. looking at a broad area all over Pisco, the area overestimated by estimation based on PALSAR imagery alone could be reestimated appropriately. That is, it would be estimated at the level of the actual severe damage ratio by using estimation based on data integration with seismic intensity data. When the model based on the Kobe earthquake was applied to Pisco without improvement, damage in the western coastal area of Pisco could not be detected [13]. The model established in this study, however, could extract damage in this area. This fact suggests that, in order to accurately estimate damage areas, it is important to use a damage extraction model suited to the target area because there are difference in urban structures, building types, and damage situations between Japan and Peru.

5. Conclusions

To develop a technology to quickly assess areas affected by earthquakes using imagery of L-band synthetic aperture radar (SAR) mounted on satellites, an estimation model of the severe damage ratio of buildings, op-

timized for Peru, has been created based on field survey data and PALSAR imagery of the city of Pisco struck by the 2007 Peru earthquake. Regression discriminant analysis has been performed in which explanatory variables, namely differences and correlation coefficients, were calculated from pre- and postearthquake PALSAR images. Target groups were six damage ranks classified based on the severe damage ratio of buildings. Examination of an optimum window size for calculation of the differences and correlation coefficients have resulted in the same parameter as that obtained from data from the 1995 Kobe earthquake. A regression discriminant function has been derived that considers urban structure, building type, the damage situation in Peru, and the pixel resolution of PALSAR imagery. Furthermore, normalized likelihood functions for the severe damage ratio have been obtained from the discriminant score of the regression discriminant function. It has also been demonstrated that the distribution of the severe damage ratio could be estimated at high accuracy based on data integration of PALSAR imagery with a fragility function based on the seismic intensity data of the Peru earthquake. Similar to PALSAR, an L-band SAR, called PALSAR-2 will be mounted on a satellite, ALOS-2, to be launched in 2013. If an earthquake occurs in Peru in the future, the model proposed in this study could be used for damage assessment. By preparing a highly reliable fragility function that fits the actual situation of buildings in Peru and integrating this with seismic intensity data based on strong-motion observation and simulation, we will be able to assess damage more accurately.

Acknowledgements

PALSAR data are the property of Japan's Ministry of Economy, Trade and Industry (METI) and the Japan Aerospace Exploration Agency (JAXA) and have been processed using the GEO Grid of the National Institute of Advanced Industrial Science and Technology (AIST). This study was supported in part by a Science and Technology Research Partnership for Sustainable Development (SATREPS) project titled Enhancement of Earthquake and Tsunami Disaster Mitigation Technology in Peru (Principal Investigator: Prof. Fumio Yamazaki); a New Energy and Industrial Technology Development Organization (NEDO) Industrial Technology Research Grant Program, titled Development of realtime tsunami damage detection technology for expeditious disaster response of Japan and ASEAN countries (Leader: Prof. Shunichi Koshimura); and a grant in aid for scientific research (Research No. 21310119; Principal Investigator: Prof. Fumio Yamazaki). We would like to express our gratitude for these contributions.

References:

[1] International Charter Space and Major Disaster, http://www. disasterscharter.org [accessed February 2012]

[2] P. Gamba, A. Marazzi, and E. Costamagna, "Satellite data analysis for earthquake damage assessment," Proc. of SPIE 3222, Earth Surface Remote Sensing (G. Cecchi, E. T. Engman, E. Zilioli (Eds.)), pp. 340-350, 1997.

[3] K. Saito, R. J. S. Spence, C. Going, and M. Markus, "Using high-resolution satellite images for post-earthquake building damage assessment: A study following the 26 January 2001 Gujarat earthquake," Earthquake Spectra, Vol.20, No.1, pp. 145-169, 2004.

[4] H. Miura and S. Midorikawa, "Distribution of building damage in the southeastern part of Beichuan county due to the 2008 Sichuan, China, earthquake based on visual detection of satellite optical images," Journal of Japan Association for Earthquake Engineering, Vol.10, No.3, pp. 46-57, 2010 (in Japanese with English abstract).

[5] S. Matsuzaki, F. Yamazaki, M. Estrada, and C. Zavala, "Visual damage interpretation of buildings using QuickBird images following the 2007 Pisco, Peru earthquake," Journal of Institute of Social Safety Science, No.13, pp. 407-413, 2010 (in Japanese with English abstract).

[6] S. Ghosh, C. K. Huyck, M. Greene, S. P. Gill, J. Bevington, W. Svekla, R. DesRoches, and R. T. Eguchi, "Crowdsourcing for rapid damage assessment: the Global Earth Observation Catastrophe Assessment Network (GEO-CAN)," Earthquake Spectra, Vol.27, No.S1, pp. S179-S198, 2011.

[7] G. A. Arciniegas, W. Bijker, N. Kerle, and V. A. Tolpekin, "Coherence- and amplitude-based analysis of seismogenic damage in Bam, Iran, using Envisat ASAR data," Transactions on Geoscience and Remote Sensing, Vol.45, pp. 1571-1581, 2007.

[8] S. Midorikawa and H. Miura, "Extraction of landslide areas due to the 2008 Iwate-Miyagi-nairiku, Japan earthquake from high-resolution SAR image," Journal of Japan Association for Earthquake Engineering, Vol.10, No.3, pp. 25-32, 2010 (in Japanese with English abstract).

[9] Y. Ito and M. Hosokawa, "An estimation model of damage degree using interferometric SAR data," IEEJ Transactions on Electronics, Information and Systems, Vol.122-C, No.4, pp. 617-623, 2002 (in Japanese with English abstract).

[10] M. Matsuoka and F. Yamazaki, "Use of satellite SAR intensity imagery for detecting building areas damaged due to earthquakes," Earthquake Spectra, Vol.20, No.3, pp. 975-994, 2004.

[11] N. Nojima, M. Matsuoka, M. Sugito, and K. Ezaki, "Quantitative estimation of building damage based on data integration of seismic intensities and satellite SAR imagery," Journal of JSCE, Division A, Vol.62, No.4, pp. 808-821, 2006 (in Japanese with English abstract).

[12] M. Matsuoka and F. Yamazaki, "Comparative analysis for detecting areas with building damage from several destructive earthquakes using satellite synthetic aperture radar images," Journal of Applied Remote Sensing, SPIE, Vol.4, 041867, 2010.

[13] M. Matsuoka and N. Nojima, "Building damage estimation by integration of seismic intensity information and satellite L-band SAR imagery," Remote Sensing, MDPI, Vol.2, No.9, pp. 2111-2126, 2010.

[14] J. S. Lee, "Digital image enhancement and noise filtering by use of local statistics," IEEE Trans. Pattern Analysis and Machine Intelligence, Vol.2, No.2, pp. 165-168, 1980.

[15] M. Estrada, C. Zavala, and Z. Aguilar, "Damage study of the Pisco, Peru earthquake using GIS and satellite images," Proceedings of International Workshop for Safer Housing in Indonesia and Peru, 2008.

[16] G. Grünthal, "European Macroseismic Scale 1998 (EMS-98)," European Seismological Commission, 1998.

[17] T. Okuno, H. Kume, T. Haga, and T. Yoshizawa, "Multivariate statistical methods," Union of Japanese Scientists and Engineers, Tokyo, Japan, pp. 259-321, 1981 (in Japanese).

[18] A. Coburn and R. J. S. Spence, "Earthquake protection – chapter 9 earthquake risk modeling –," John Wiley & Sons, p. 436, 2002.

[19] K. A. Porter, K. S. Jaiswal, D. J. Wald, M. Greene, and C. Comartin, "WHE-PAGER project: a new initiative in estimating global building inventory and its seismic vulnerability," Proc. The 14th World Conference on Earthquake Engineering, No.S23-016, 2008.

[20] US Geological Survey, "ShakeMap," http://earthquake.usgs.gov/eqcenter/shakemap/ [accessed February 2012]

[21] US Geological Survey, "ShakeMap us2007gbcv," http://earthquake.usgs.gov/eqcenter/shakemap/global/shake/2007gbcv/ [accessed June 2009]

[22] K. Fujimoto and S. Midorikawa, "Empirical method for estimating J.M.A. instrumental seismic intensity from ground motion parameters using strong motion records during recent major earthquakes," Journal of Institute of Social Safety Science, No.7, pp. 214-246, 2005 (in Japanese with English abstract)

Name:
Masashi Matsuoka

Affiliation:
Associate Professor, Department of Built Environment, Tokyo Institute of Technology

Address:
Nagatsuta 4259-G3-2, Midori-ku, Yokohama 226-8502, Japan

Brief Career:
1992 Research Associate, Tokyo Institute of Technology
1996 Engineer, Remote Sensing Technology Center of Japan
1998 Deputy Team Leader, RIKEN
2004 Team Leader, National Research Institute for Earth Science and Disaster Prevention
2007 Senior Research Scientist, National Institute of Advanced Industrial Science Technology
2010 Division Chief, National Institute of Advanced Industrial Science Technology
2012- Associate Professor, Tokyo Institute of Technology

Selected Publications:
- Matsuoka and Yamazaki, "Use of Satellite SAR Intensity Imagery for Detecting Building Areas Damaged due to Earthquakes," Earthquake Spectra, EERI, Vol.20, No.3, pp. 975-994, 2004.
- Matsuoka and Nojima, "Building Damage Estimation by Integration of Seismic Intensity Information and Satellite L-band SAR Imagery," Remote Sensing, MDPI, Vol.2, No.9, pp. 2111-2126, 2010.
- Matsuoka and Yamazaki, "Comparative Analysis for Detecting Areas with Building Damage from Several Destructive Earthquakes Using Satellite Synthetic Aperture Radar Images," Journal of Applied Remote Sensing, SPIE, Vol.4, 041867, 2010.

Academic Societies & Scientific Organizations:
- Earthquake Engineering Research Institute (EERI)
- Architectural Institute of Japan (AIJ)
- Remote Sensing Society of Japan (RSSJ)

Name:
Miguel Estrada

Affiliation:
General Director, CISMID
Associate Professor, Faculty of Civil Engineering, National University of Engineering

Address:
Av. Tupac Amaru 1150, Rimac, Lima, Peru

Brief Career:
1998-2000 Master of Engineering in the field of Civil Engineering, The University of Tokyo
2000-2004 Ph.D. of Civil Engineering, The University of Tokyo
2004-present Associate Professor, Faculty of Civil Engineering, National University of Engineering
2013-present General Director, Japan-Peru Center for Earthquake Engineering Research and Disaster Mitigation (CISMID), Faculty of Civil Engineering, National University of Engineering

Selected Publications:
- M. Estrada, H. Miura, F. Yamazaki, and S. Midorikawa, "Evaluation of Social Seismic Vulnerability through High Resolution Satellite Imagery," 15th World Conference on Earthquake Engineering, Portugal, 2012.
- M. Estrada, C. Zavala, and Z. Aguilar, "Use of Geomatics for Disaster Management – Case Study 2007 Peru, Pisco Earthquake," 7th International Workshop on Remote Sensing and Disaster Response, USA, 2009.
- M. Estrada, M. Matsuoka, and F. Yamazaki, "Use of Optical Satellite Images for the Recognition of Areas Damaged by Earthquakes" 6th International Conference on Seismic Zonation, USA, 2000.

Academic Societies & Scientific Organizations:
- Peruvian Board of Engineers
- Earthquake Engineering Research Institute